BEAM DYNAMICS IN THE SPALLATION NEUTRON SOURCE LINAC*

D. Jeon# representing the SNS Project, Oak Ridge, Tennessee, USA

Abstract

Being an 1.44MW machine, the beam loss requirement on the SNS linac is less than 1W/m and controlling halo particle generation is of great importance. Beam dynamics aspects of the SNS linac design are presented considering various halo generation mechanisms. A halo generation mechanism in the non-periodic lattices such as the SNS linac MEBT (Medium-Energy Beam-Transport between RFQ and DTL) is reported. We find that the nonlinear space charge force resulting from large transverse beam eccentricity ~2:1 in the ~1.6-m-long MEBT chopper section is responsible for halo formation [1]. The proposed mitigation measures are modifying the MEBT optics and introducing adjustable collimators in the MEBT. The transient beam behavior of the LEBT and MEBT choppers is also studied for the fate of partially chopped beams.

INTRODUCTION

The SNS (Spallation Neutron Source) accelerator system is designed to accelerate intense proton beams to energy of 1-GeV, delivering more than 1.4 MW (upgradeable to 2 MW) of beam power to the neutron production target [2]. The peak current in the linac is 38mA and the macropulse average current is 26mA. The SNS linac has the following structure; ion source, LEBT (Low-Energy Beam-Transport), RFQ (Radio-Frequency Quadrupole), MEBT (Medium-Energy Beam-Transport), DTL (Drift Tube Linac), CCL (Coupled Cavity Linac), and SCL (SuperConducting Linac). A primary concern is potential damage and radio activation of accelerator components resulting from uncontrolled beam losses. A major source of loss is beam halo that intercepts the bore of the linac.

First, beam dynamics aspects of the SNS linac design are presented. A new halo mechanism and its mitigation scheme are presented. The transient beam behavior of the LEBT and MEBT choppers is also presented, which shows significant emittance growth.

BEAM DYNAMICS DESIGN

Aspects of the SNS linac design have been reported [3]. The following lists the conditions imposed to avoid or minimize halo generation:

- Avoid envelope instabilities by keeping zero current phase advance below 90°.
- Minimizing space charge coupling resonance crossing.
- Making phase advance per unit length continuous for current independence.

We selected focusing lattice parameters to avoid envelope instabilities throughout the linac. The zero current phase advance per period σ_{ot} and σ_{ol} never exceeds 90° as in Fig. 1. We avoid the 1:1 parametric resonance by adjusting quadrupole gradients so that σ_{ot} and σ_{ol} do not cross except in the DTL tank 1 and CCL module 4 where matching considerations take precedence.

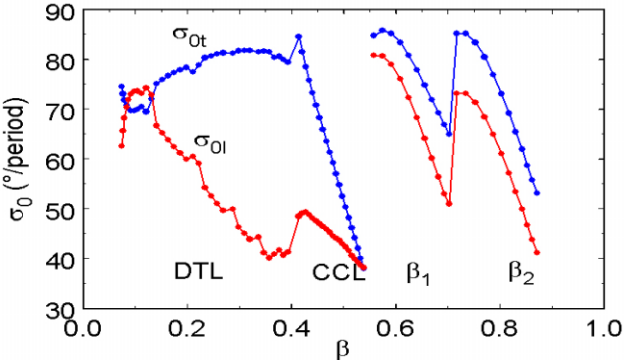

Figure 1: Phase advance is below 90° and resonance crossing is minimized.

Figure 2 is a resonance chart for the nominal SNS design parameter, which includes a 52mA beam current and an emittance ratio $\varepsilon_z/\varepsilon_x$ of 1.2. The contoured peaks identify space charge coupling resonances. The shaded contours indicate the expected rates of emittance growth with 5% being the lowest value plotted. The two peaks on the left side represent weak coupling resonances that take a long time to develop (3:1 and 2:1). This indicates that space charge coupling resonance poses little risk for the current SNS linac design. Vertical axis is tune depression and horizontal axis is the tune ratio between transverse and longitudinal dimension.

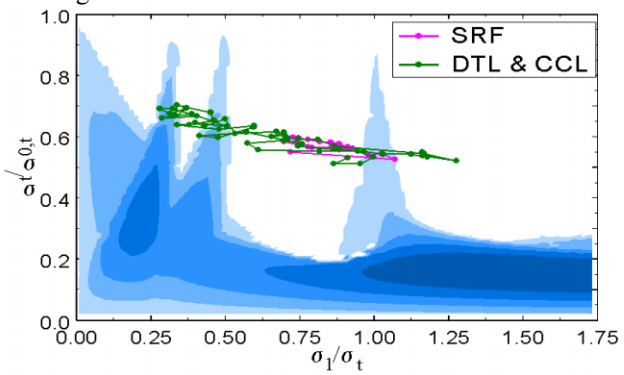

Figure 2: The SNS linac tune trajectory on the resonance chart.

We make k_{ot} and k_{ol}, the phase advance per unit length continuous across all lattice transitions as shown in Fig. 3. This design feature minimizes the potential for

* SNS is managed by UT-Battelle, LLC, under contract DE-AC05-00OR22725 for the U.S. Department of Energy.
#jeond@ornl.gov

mismatches and helps assure a current independent design.

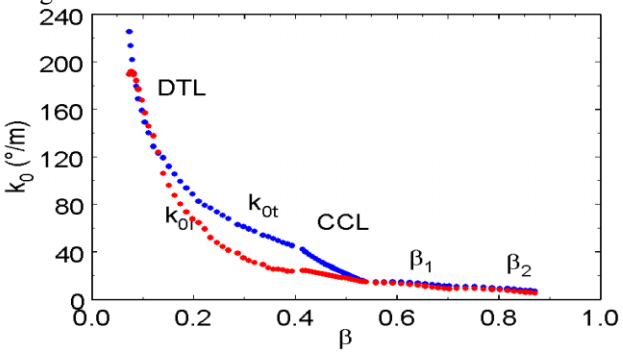

Figure 3: Phase advance per unit length is continuous.

HALO GENERATION MECHANISM

Beam dynamics simulations of the SNS linac show that the beam halo develops at low energy, but some halo particles survive acceleration to higher energies before being lost primarily on the CCL bore as shown in Fig. 4. This particle loss at higher energies results in radio activation of the CCL. In order to find ways to mitigate this halo related beam loss, we conducted studies to identify the sources and mechanism of halo formation. It turns out that the MEBT is the largest contributor to FE halo generation in the SNS linac [1].

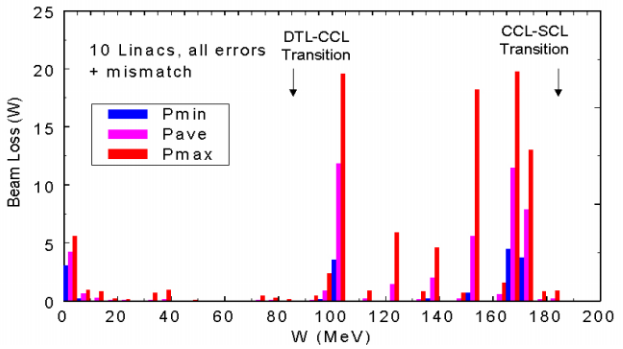

Figure 4: Beam loss along the SNS linac.

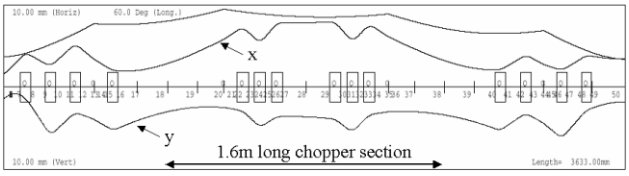

Figure 5: Trace3D beam envelope profiles of MEBT.

To better understand MEBT optics, the horizontal (x curve) and vertical (y curve) envelope profiles of the sqrt(5) * rms beam size in the MEBT are plotted in Fig. 5. The top curve is longitudinal envelope profile. The beam is squeezed vertically to clear the vertical deflection plates of both the chopper and anti-chopper and relaxed horizontally. This arrangement is necessary to have 90° zero-current betatron phase advance between the chopper box and the chopper target in the middle, and between the chopper target and the anti-chopper box as well. However, this 1.6-m-long chopper section with a large beam eccentricity is the source of halo formation.

Figure 6 shows the electric field (in arbitrary unit) on top of real space projections of beam distribution at the chopper target (in the middle of the MEBT) where the beam eccentricity is ~2:1. The beam is wide in x and narrow in y. The Ex becomes nonlinear beyond x=0.5 cm, which is well inside the core. This means that the outer part of core with |x| > 0.5 cm (marked as "potential halo") is subject to nonlinear space charge force and their phase advance is quite different from the inner part of the core seeing linear space charge force. The phase advance difference over the 1.6-m chopper section leads to severe beam distortion in horizontal phase space. In the case of Ey, only small fraction of halo particles sees nonlinear space charge force. This is why the tail develops mainly in x phase space by the end of the MEBT.

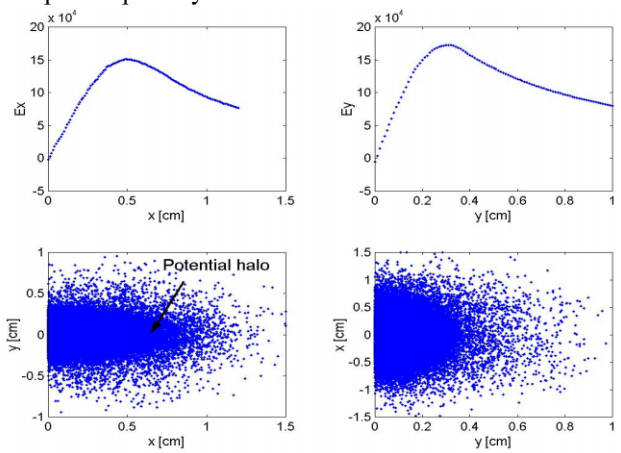

Figure 6: Plots of E field and real space projections of beam distribution. The unit of E field is arbitrary. x rms beam size is 3.40mm and y rms beam size 1.71 mm.

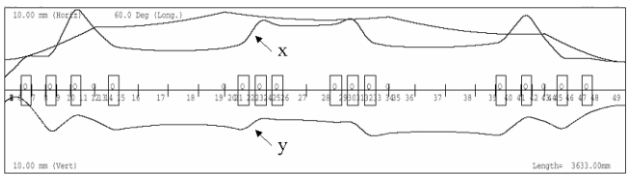

Figure 7: Trace3D envelope profiles of round beam optics.

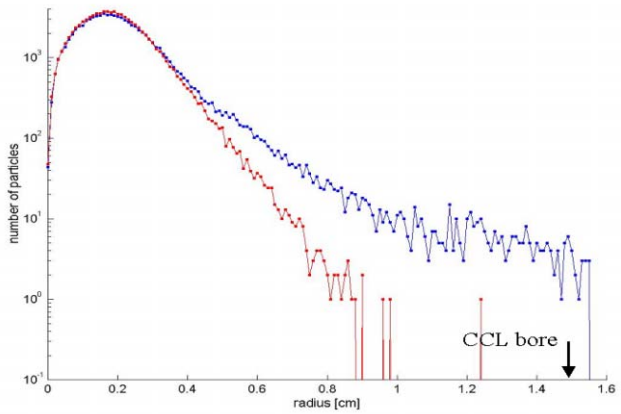

Figure 8: radial beam profile at 171MeV before (the blue curve, baseline case) and after the MEBT optics change alone (the red curve).

To suppress halo formation induced by large transverse beam eccentricity, the optics of lattices should make the beam as round as possible. For the purpose of studying, we modified the entire MEBT optics to reduce beam eccentricity as shown in Fig. 7 (compare with Fig. 5).

Making the beam round indeed suppresses the halo formation as shown in Fig. 8 that depicts the beam profiles at 171 MeV before and after optics modification. However, modification of the entire MEBT optics is not viable to facilitate the beam chopping for ring injection. At least the first half of the MEBT should not be modified, while the second half can be modified.

HALO MITIGATION SCHEME

A hybrid scheme is adopted for halo mitigation that is a combination of alternative MEBT optics and adjustable collimators at the MEBT chopper target.

Alternative MEBT optics

In an alternative design, the upstream half of MEBT optics is preserved while the downstream half of MEBT optics is modified for round beam. The resulting beam cross section is more circular as shown in Fig. 9. Now, the anti-chopper no longer restores a partially chopped portion of the beam to its original (on-axis) position in phase space, if indeed that were desirable. Also, the beam now has a larger vertical extent and approaches the anti-chopper plates as designed.

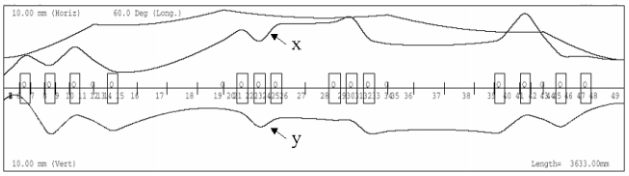

Figure 9: The proposed alternative MEBT optics.

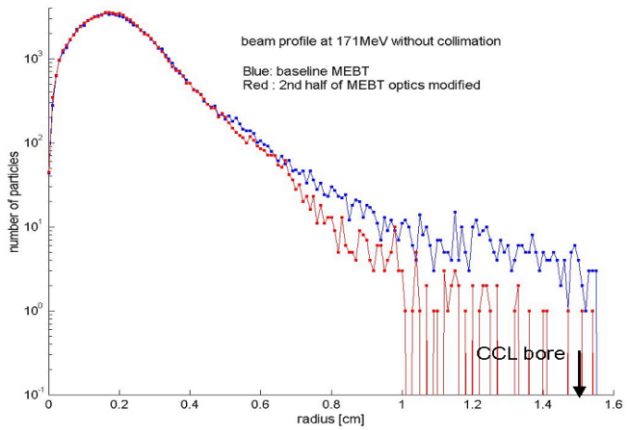

Figure 10: Radial beam distribution at 171MeV for the baseline MEBT optics without collimation (the blue curve) and for the alternative MEBT optics without collimation (the red). 87% of the beam tail with r > 9 mm is removed just due to optics change.

This simple modification to the optics alone reduces the formation of transverse tails substantially and improves the beam quality in the downstream linac. Figure 10 shows that 87% of the beam tails with r > 9 mm at 171MeV is removed (compared with the blue curve).

MEBT scraping

There are only a few places where collimators will fit in the MEBT. One convenient place is at the chopper target. Figure 11 shows the layout of the MEBT with the chopper target and anti-chopper box indicated by arrows. A pair of adjustable horizontal collimators would be installed in the chopper target box (at the red arrow). The chopper target itself is located above the mid-plane to intercept beam that is deflected upward. Collimators mounted on horizontal actuators will not interfere with the function of the target.

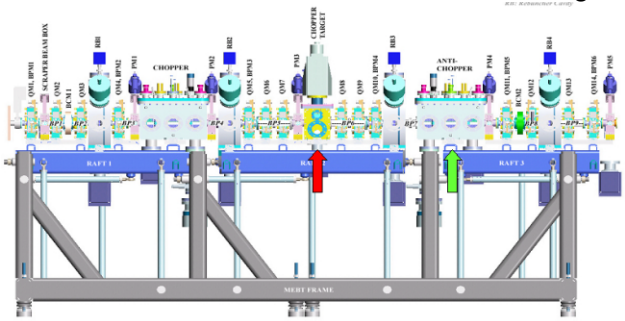

Figure 11: Schematic layout of MEBT indicating the location of adjustable collimators.

This assembly is shown schematically in Fig. 12. This collimator implementation has the advantage that it is readily adjustable to accommodate the actual beam conditions, which are expected to vary with different operating conditions such as beam current, ion-source performance, LEBT, RFQ, and MEBT tuning. The other advantage is that the proposed collimators can be cooled easily. The adjustable collimators are designed to scrape up to about 20% of beam power when they are made of Carbon/Carbon composite [4].

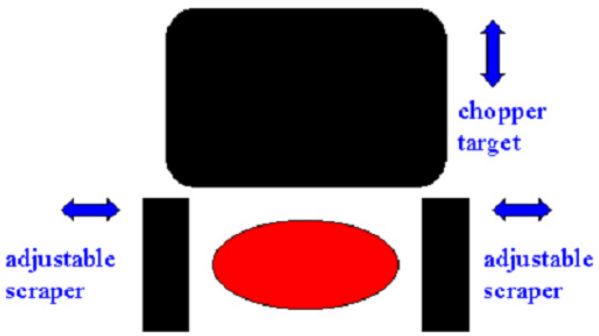

Figure 12: Schematic drawing of adjustable collimators and the chopper target.

Figure 13 shows the radial beam distribution at 171 MeV resulting from this hybrid solution, which combines the alternative MEBT optics and the MEBT scraping at the chopper target. 97% of the halo with r > 9 mm is removed compared with the baseline case (in blue). Even for the increased peak current of 54mA rather than 38mA, there is also an enough safety margin even for this case.

With the adopted mitigation scheme, we expect to reduce uncontrolled beam loss associated with halo to a manageable level.

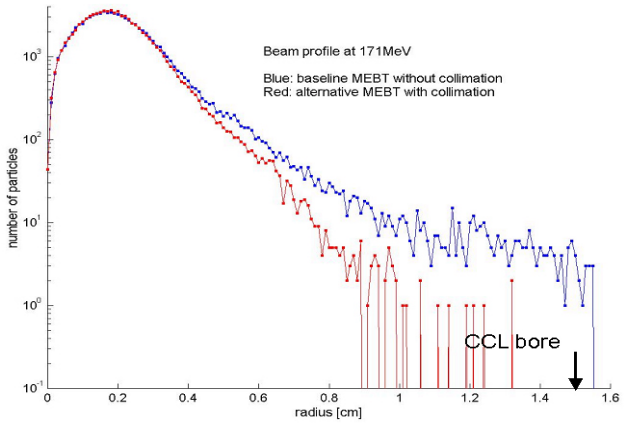

Figure 13: Radial beam profile at 171MeV for the adopted hybrid scheme mitigating halo (red curve).

TRANSIENT BEAM BEHAVIOR

Detailed analysis of transient beam behavior of LEBT and MEBT choppers was performed [5]. The beam duty factor of the SNS linac is 6%: 1-ms macropulses at 60 Hz. The chopping breaks each macropulse into 1060 minipulses separated by 300-ns gaps for ring extraction, thus passing 68% of the beam as illustrated in Fig. 14.

Chopping is done in two stages: LEBT chopper and MEBT chopper. The LEBT chopper deflects the beam into the RFQ, and the MEBT chopper deflects beam vertically onto the chopper target. Because of the several-ns rise and fall time of the chopper voltage, the edges of the beam gap are "contaminated" with partially chopped micropulses whose destiny is of interest.

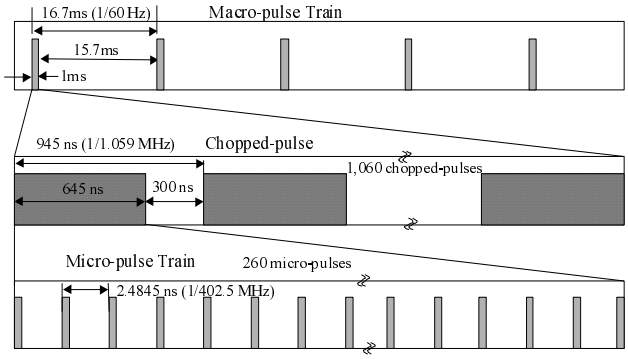

Figure 14. Time structure of the SNS beam-pulses.

LEBT chopper

The LEBT chopper is a segmented Einzel lens as shown at left in Fig. 15. This segmented electrode is just upstream of the grounded entrance aperture of the RFQ at far right in the figure.

Collectively, the four chopper electrodes operate at -40 kV to focus the beam into the RFQ. By superimposing ±2 kV on opposing segment pairs we can arrange to deflect the beam toward 45°, 135°, 225°, or 315°. During a 300-ns chopping gap, the electrodes maintain a constant orientation. For a voltage rise and fall time of 25 ns, up to 20 micropulses in each gap may experience only partial deflection. Operating in the chopping mode breaks axial symmetry the of LEBT fields. For our beam simulation studies, we transport the beam through the 3-D fields of the LEBT.

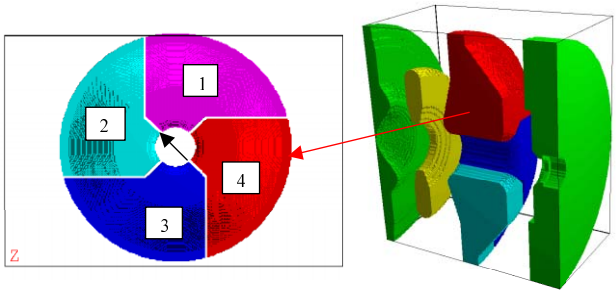

Figure 15: LEBT chopper configuration.

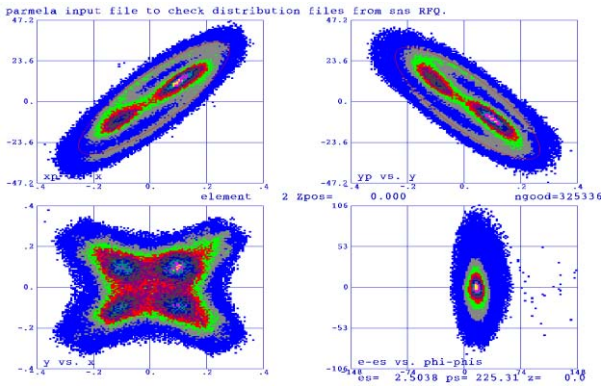

Figure 16: Superimposed phase-space distributions at the RFQ-exit for 4 partially LEBT-chopped beams.

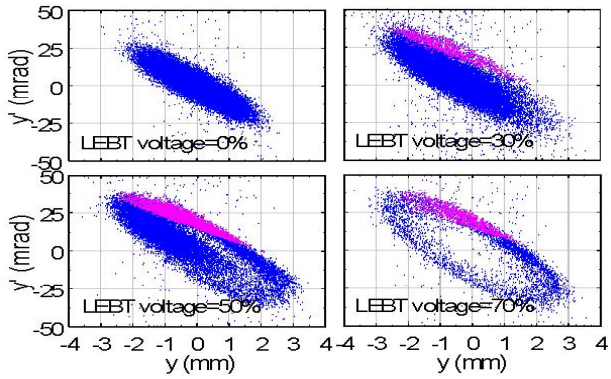

Figure 17: Phase space (y-y') projections at the RFQ exit for different LEBT voltages.

With the chopper off, the beam arrives "matched" at the RFQ entrance. When the LEBT chopper is on, the beam enters the RFQ off-axis and off-angle. This off axis beam results in significant emittance growth at its exit as shown in Fig. 16.

Figure 17 shows the evolution of the y-y' phase space of this beam at the RFQ exit during the LEBT voltage ramp at 0%, 30%, 50% and 70% of maximum deflection into the first quadrant. Blue dots represent particles that have survived the RFQ. During the ramp, we see about ten-fold increase in emittance and the y-y' projection

transforms to a hollow ellipse. Red dots represent the particles at the RFQ output that survived the MEBT chopper at its full voltage and appear at the entrance to the DTL. These particles represent potential contamination of the edges of the chopper gap.

MEBT chopper

Figure 18 shows the y-y' emittance at the DTL entrance for four voltages of MEBT acting alone. The asymmetry of the unchopped beam reflects the missing 1% removed by the chopper target. During the MEBT transient, the beam entering the linac nominally remains within the phase space defined by the matched beam. However, even at full chopper voltage ~16 μA (peak) enters the linac, which fails to meet the gap-current goal, when MEBT chopper acting alone. Nonetheless, the remnant of the beam is well within the acceptance of the SNS linac.

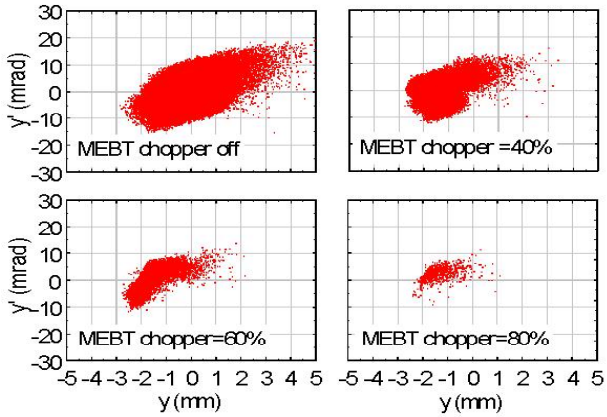

Figure 18: Particle coordinates (y-y') at the DTL input for various MEBT chopper voltage when acting alone.

We consider four different chopper-timing sequences that are illustrated in Fig. 19. The left-hand column shows the relative timing between the LEBT chopper (in red) and the MEBT chopper (in blue) and the voltage ramps of the two choppers. The middle column shows the corresponding current in individual micropulses at the entrance to the DTL, assuming a linear relationship between voltage and beam current chopped. The right-hand column shows the current intercepted on the MEBT-chopper target during the turn-on transient. Table 1 summarizes the relative virtues of the four options in Fig. 18. To test the linear model we simulated the performance for option 1 using 10^6 macroparticles.

Option 3 is most attractive because it minimizes the potential beam loss in the linac while easily meeting the chopper-target power limitations. Partially chopped beam lost at or near the DTL entrance corresponds to less than 0.1 W, meeting the beam-loss limit of 1 W/m. With both choppers at full voltage, only ~31 nA peak current (1.2x 10^{-5}) enters the DTL, easily meeting the gap cleanliness requirement of 10^{-4}.

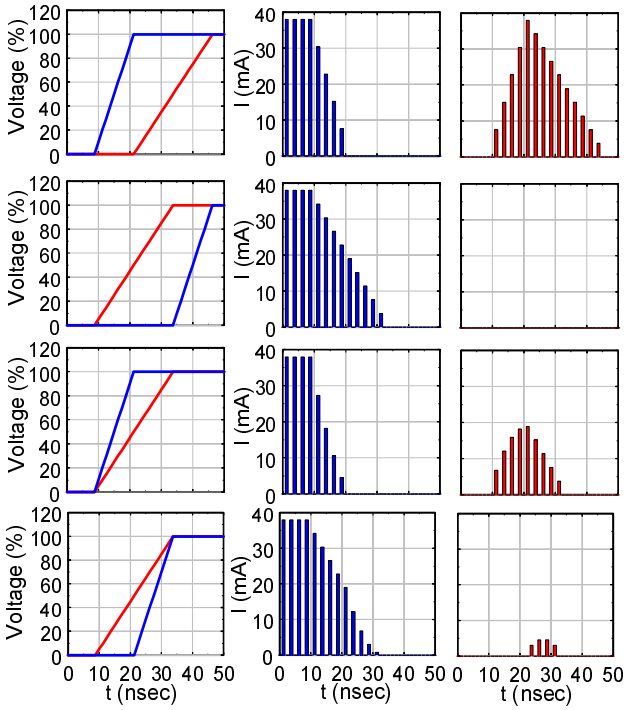

Figure 19: Chopper timing options showing LEBT and MEBT voltage ramps, micropulse current in the falling edge of the chopper gap and micropulse current on the chopper target.

Table 1: Linear model predictions and simulation.

chopper timing option	average linac current during transient	average MEBT target power dissipation
	(μA)	(W)
1	24	226
2	54	0
3	19	87
4	49	12
simulation	16	208

REFERENCES

[1] D. Jeon et al, Phys. Rev. ST Accel. Beams **5**, 094201 (2002).

[2] J. Wei et al, Proceedings of the 2001 Part. Accel. Conf. (Chicago, 2001), p. 319.

[3] J. Stovall et al, Proceedings of the 2001 Part. Accel. Conf. (Chicago, 2001), p. 446.

[4] Private communication with S. Kim: Carbon/Carbon is considered developed for the fusion reactor is. See http://www.toyotanso.com.

[5] S. Nath et al, Proceedings of the 2002 LINAC Conf. (Gyongju, S. Korea, 2002), p. 319.